ChemSusChem

Research Article
doi.org/10.1002/cssc.202102217

Chemistry Europe
European Chemical Societies Publishing

www.chemsuschem.org

Identifying UiO-67 Metal-Organic Framework Defects and Binding Sites through Ammonia Adsorption

Venkata Swaroopa Datta Devulapalli[+],[a] Ryan P. McDonnell[+],[a, d] Jonathan P. Ruffley,[b] Priyanka B. Shukla,[b] Tian-Yi Luo,[c] Mattheus L. De Souza,[c] Prasenjit Das,[c] Nathaniel L. Rosi,[c] J. Karl Johnson,*[b] and Eric Borguet*[a]

Ammonia is a widely used toxic industrial chemical that can cause severe respiratory ailments. Therefore, understanding and developing materials for its efficient capture and controlled release is necessary. One such class of materials is 3D porous metal-organic frameworks (MOFs) with exceptional surface areas and robust structures, ideal for gas storage/transport applications. Herein, interactions between ammonia and UiO-67-X (X: H, NH_2, CH_3) zirconium MOFs were studied under cryogenic, ultrahigh vacuum (UHV) conditions using temperature-programmed desorption mass spectrometry (TPD-MS) and in-situ temperature-programmed infrared (TP-IR) spectroscopy. Ammonia was observed to interact with μ_3–OH groups present on the secondary building unit of UiO-67-X MOFs via hydrogen bonding. TP-IR studies revealed that under cryogenic UHV conditions, UiO-67-X MOFs are stable towards ammonia sorption. Interestingly, an increase in the intensity of the C–H stretching mode of the MOF linkers was detected upon ammonia exposure, attributed to NH–π interactions with linkers. These same binding interactions were observed in grand canonical Monte Carlo simulations. Based on TPD-MS, binding strength of ammonia to three MOFs was determined to be approximately 60 kJ mol^{-1}, suggesting physisorption of ammonia to UiO-67-X. In addition, missing linker defect sites, consisting of H_2O coordinated to Zr^{4+} sites, were detected through the formation of $n NH_3{\cdot}H_2O$ clusters, characterized through in-situ IR spectroscopy. Structures consistent with these assignments were identified through density functional theory calculations. Tracking these bands through adsorption on thermally activated MOFs gave insight into the dehydroxylation process of UiO-67 MOFs. This highlights an advantage of using NH_3 for the structural analysis of MOFs and developing an understanding of interactions between ammonia and UiO-67-X zirconium MOFs, while also providing directions for the development of stable materials for efficient toxic gas sorption.

Introduction

On a global scale, more than 200 million tons of NH_3 are produced and consumed annually in the synthesis of commercial materials, such as fertilizers, additives in refrigerants, and so on.[1] Recent reports highlight the potential of NH_3 as an alternative clean-burning fuel, owing to its high hydrogen density and release of nontoxic byproducts upon combustion.[2] Moreover, NH_3 has applications in several fields, for example, infrared spectroscopy, as an acidic site probe,[3] and metallurgy, as a lixiviant.[4] Despite its useful properties, NH_3 is toxic and highly corrosive, thus requiring efficient materials for its storage/transport.

Materials initially considered for NH_3 sorption included carbon-based materials, such as activated carbon and carbon nanotubes. Studies performed on single-wall carbon nanotubes (SWCNTs) by Feng et al. reveal not only the impact of functional groups on sorption but also the importance of sorbent pretreatment procedures to maximize NH_3 sorption.[5] However, it was also reported that pristine and defective (missing carbon) SWCNTs showed weak adsorption of NH_3 and that SWCNTs had to be refluxed in an acidic environment to enhance the uptake of NH_3.[5] Due to these limitations, porous organic materials, which have higher surface areas and porosities than SWCNTs, have been investigated for their ability to capture NH_3. In addition to higher surface areas, these porous materials offer several advantages over SWCNTs, such as post synthetic modifications, tunable porosities, pore environment optimization, and others, making them promising candidates for optimal gas sorption/separation.[6]

Porous organic polymers are built using strong covalent bonds, which have high chemical and thermal stability.[7] A study on NH_3 adsorption by porous organic polymers revealed the affinity of NH_3 to Brønsted acidic sites over Lewis acidic sites and reported excellent capacity for NH_3.[8] However, the study

[a] V. Swaroopa Datta Devulapalli,[+] R. P. McDonnell,[+] Prof. E. Borguet
Department of Chemistry
Temple University
Philadelphia, PA 19122 (USA)
E-mail: eborguet@temple.edu
[b] Dr. J. P. Ruffley, P. B. Shukla, Prof. J. Karl Johnson
Department of Chemical and Petroleum Engineering
University of Pittsburgh
Pittsburgh, PA 15261 (USA)
E-mail: karlj@pitt.edu
[c] Dr. T.-Y. Luo, M. L. De Souza, Dr. P. Das, Prof. N. L. Rosi
Department of Chemistry
University of Pittsburgh
Pittsburgh, PA 15261 (USA)
[d] R. P. McDonnell[+]
Present Address:
Department of Chemistry
University of Wisconsin – Madison
Madison, WI 53706 (USA)
[+] These authors contributed equally to this work.

Supporting information for this article is available on the WWW under https://doi.org/10.1002/cssc.202102217

also concluded that merely increasing the density of Brønsted acidic groups does not enhance the NH_3 sorption capacity, which is dependent on other factors (e.g., humidity).[8] In addition, porous organic polymers are challenging to synthesize without the densely packed Brønsted acid groups blocking the pores, leading to reduced NH_3 sorption. This drawback has motivated the search for materials with better capability to capture NH_3.

Over the past decade, zirconium-based metal-organic frameworks (MOFs), particularly the UiO family, have displayed superior thermal, mechanical, and chemical stabilities compared to other MOFs.[9] First synthesized by Lillerud and co-workers in 2008, Zr UiO MOFs exhibited several advantages over other MOFs, attributable to strong Zr-carboxylate bonds between the metal node and MOF linker.[10] Ideally, UiO-67 MOFs consist of Zr_6 nodes interconnected with 12 biphenyldicarboxylate (BPDC) linkers, which results in the formation of a framework with two different pore geometries: tetrahedral and octahedral. These materials are suitable for the sorption of various simple molecules (e.g., CH_4, N_2, CO_2), toxic gases (e.g., NO_2, SO_2),[11] and the catalytic degradation of chemical warfare agents and their simulants.[12] Moreover, strategically engineered defects created through pretreatment methods are reported to influence the stability and sorption properties of UiO-67 MOFs.[13]

Ex-situ/bulk characterization techniques, such as breakthrough experiments and X-ray diffraction, can, respectively, reveal the total capacity or post exposure stability of the sorbent, but do not convey real-time information on the interactions between the sorbate and the sorbent.[14] In-situ analysis, crucial for determining sorbate-sorbent interactions, assists in the development of superior sorbent materials. Hence, we examine NH_3 sorption on UiO-67-X using in-situ temperature-programmed infrared spectroscopy (TP-IR) and temperature-programmed desorption mass spectrometry (TPD-MS) under ultrahigh vacuum (UHV) at cryogenic temperatures, in order to eliminate atmospheric contaminants and explicitly analyze NH_3-UiO-67 interactions.[15] The substituent functional groups on the linkers are chosen to understand the effects of polar (NH_2) and non-polar (CH_3) groups on NH_3 sorption. Using in-situ Fourier-transform infrared (FTIR) spectroscopy, we characterize a novel phenomenon of interactions of NH_3 with the linker groups and show that, under UHV conditions, NH_3 sorption is completely reversible, confirmed by relatively small binding energies computed through TPD-MS. These phenomena have been confirmed through the identification of a corresponding local energy minimum with density functional theory (DFT) calculations and grand canonical Monte Carlo (GCMC) simulations. In addition, we successfully probe missing linker defects (where zirconium coordination is satisfied by H_2O molecules and charge is balanced by OH^- ions) in UiO-67 MOFs using in-situ IR spectroscopy and show that thermal activation to successively higher temperatures results in a decrease of these moieties.

Results and Discussion

IR spectra of MOFs prior to NH_3 adsorption are similar to that of pristine UiO-67 samples previously reported.[16] Experimental and simulated N_2 isotherms (77 K) were compared to assess the sample quality (Figure S1d). The similarity in profiles and uptake capacities indicate minimally defective UiO-67 MOFs.[17] The N_2 isotherms show a stark contrast to those of defective UiO-67 samples,[18] further suggesting pristine samples of UiO-67.

In-situ infrared spectroscopy

Upon 5000 L NH_3 exposure (1 L = Langmuir = 10^{-6} Torr s), significantly less than required to saturate the material, several bands characteristic of NH_3 evolve in the 3400–3200 and 1700–900 cm^{-1} regions (Figures 1 and S4, respectively). The broad bands in the 3200–3400 cm^{-1} region are assigned to symmetric [$\nu(NH)_{sym}$] and asymmetric [$\nu(NH)_{asym}$] N–H stretching and $2\delta(NH_3)_{asym}$ of condensed-phase NH_3.[19] Bands situated at around 3335 and 3400 cm^{-1} are indicative of $\nu(NH)_{sym}$ and $\nu(NH)_{asym}$ of gas-phase NH_3, respectively, likely due to NH_3 confined within the UiO-67 framework.[5,20] In addition, a band at around 1060 cm^{-1} (Figure S5), associated with the NH_3 umbrella mode, is further evidence of condensed-phase NH_3 adsorbed on MOF.[21] The assignments of significant peaks in the IR spectra, obtained from NH_3 adsorption on MOF and a comparison to adsorption on other porous materials, are summarized in Tables SI1 and SI2.

In addition to observing vibrational modes of condensed- and gas-phase NH_3, the IR spectra reveal that NH_3 interacts with both the MOF node and linker. After NH_3 adsorption (Figure 1), a decrease in the μ_3–OH stretching mode [$\nu(OH)_{free}$] at around 3680 cm^{-1} is detected and a band corresponding to $\nu(OH)_{HB}$ appears at around 3200 cm^{-1}. These phenomena are attributed to NH_3 hydrogen bonding with μ_3–OH groups present on the node via the lone pair on the ammonia nitrogen.[22] This result

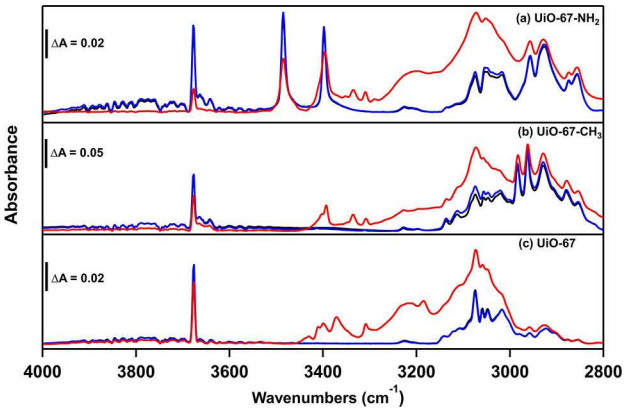

Figure 1. FTIR spectra of (a) UiO-67-NH_2, (b) UiO-67-CH_3, and (c) UiO-67 showing initial spectra of MOF before exposure (black), 5000 L NH_3 adsorbed on MOF (red), and MOF after thermal treatment (blue) in the 4000–2800 cm^{-1} region. UiO-67, UiO-67-NH_2 activated to 473 K; UiO-67-CH_3 activated to 423 K. Spectra acquired at 100 K.

was confirmed with DFT, which showed that the μ_3–OH is an energetically favorable binding site for NH_3 (Figure 2). An NH_3–μ_3–OH binding energy of $-68\ kJ\,mol^{-1}$ was obtained via Equation (1); the H_3N–HO bond length is approximately 1.74 Å, consistent with strong hydrogen bonding:

$$\Delta E_{bind} = E_{MOF+analyte} - E_{analyte} - E_{MOF} \quad (1)$$

Despite the modes indicative of NH_3 adsorption, several features present in Figure 1 [e.g., the increase in ν(CH) intensity] are not intrinsic to gaseous or condensed-phase NH_3, suggesting some other type of interaction between NH_3 and the MOF linker. The intensity of the MOF intrinsic ν(CH), around 3050 cm^{-1}, increases significantly upon NH_3 adsorption, as seen in Figure 1. Additionally, a band approximately 1350 cm^{-1} is seen upon NH_3 adsorption to UiO-67 (Figure S5), similarly seen in NH_3 adsorption upon SWCNTs.[23] These bands are possibly indicative of the presence of ammonia clusters, $(NH_3)_n$. However, the expected cluster IR signatures (i.e., features near 3241 and 3321 cm^{-1}) are not evident in spectra of NH_3 adsorption on UiO MOFs (Figures 1 and 4), and thus the increase in intensity at around 3050 cm^{-1} cannot be attributed to the formation of $(NH_3)_n$ clusters.[24] Instead, we hypothesize that NH_3 adsorption causes a perturbation of the π system of the MOFs via its H atoms, enhancing the intensity of the linker's ν(CH) vibrational modes.

It has been reported that some molecules can undergo an interaction similar to hydrogen bonding with an aromatic π system. In the case of NH_3, it is observed that NH_3 typically forms hydrogen bonds with π systems through its hydrogen atoms, and not through its lone pair, resulting in an NH–π interaction.[25] This phenomenon has been reported for single NH_3 molecule interactions with benzene[26] and phenylacetylene.[27] Similar interactions were also observed between NH_3 and SWCNTs, demonstrating the occurrence of NH–π interactions in porous materials as well.[23]

Thus, the increase in the ν(CH) intensity and the blueshift in the NH_3 umbrella motion frequencies are hypothesized to be due to NH–π interactions. These interactions are theoretically predicted in van der Waals clusters (e.g., benzene and NH_3, phenylacetylene and NH_3), and experimentally shown through NH_3 adsorbed upon SWCNTs, but not reported in the case of MOFs.[23,26–28] The main source of π bonding/interacting groups in MOFs are linkers. Probe–linker interactions, if present, are not readily observed and are seldom reported.[29] To the best of our knowledge, this is the first experimental evidence, using IR spectroscopy, of this peculiar phenomenon of NH–π interactions and enhancement in the ν(CH) intensity of a MOF. The ν(CH) intensity enhancement possibly occurs due to a reduction in linker symmetry via the NH–π interaction, causing typically non-IR active modes to become IR active.[30]

We confirmed the presence of NH–π interactions with DFT, observing a binding energy of $-11.8\ kJ\,mol^{-1}$ for the configuration shown in Figure 3. It is also shown that, while interacting with the linker π system through its hydrogen atoms, NH_3 interacts with other MOF moieties via its lone pair (Figure S3). Hence, as proposed for NH_3 adsorption on SWCNTs, steric effects are hypothesized to be a probable cause for the increase in ν(CH) intensity and blueshift in the umbrella modes.[23] To this end, we provide a DFT calculated structure, which shows NH_3 at sites near the node in the octahedral pore (Figure S3), as reported by Yoskamtorn et al. experimentally.[18b] This structure shows interaction with both the aromatic rings and the MOF node, with the interaction being primarily driven by electrostatics.[31] There is also a possibility NH_3 interacts with the linker π systems through its hydrogen atoms while simultaneously interacting at the μ_3–OH site (Figure 2) with its lone pair. Simulated IR spectra at the PBE-D3/6-31G(d) level of theory reveal the emergence of additional ν(CH) bands when NH_3 interacts with the BPDC linker (Figure S8), but, contrary to experimentally observed results, the calculations show an overall decrease in intensity. Since the calculations are performed on simplified models and not on NH_3 within the

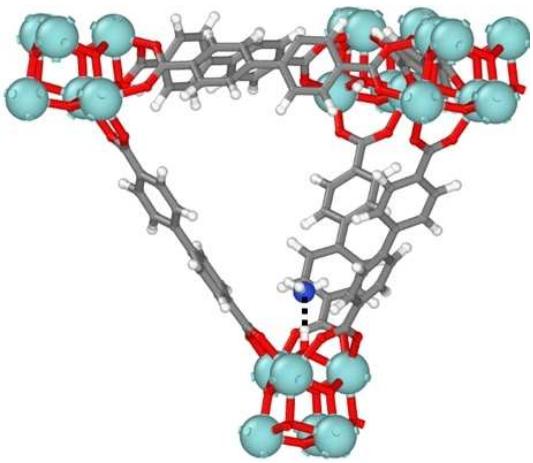

Figure 2. Interaction of a single NH_3 molecule at the μ_3–OH site of UiO-67, obtained through DFT calculations. $\Delta E_{bind} = -68\ kJ\,mol^{-1}$; the H_3N–HO bond length, shown as the dashed line, is 1.74 Å.

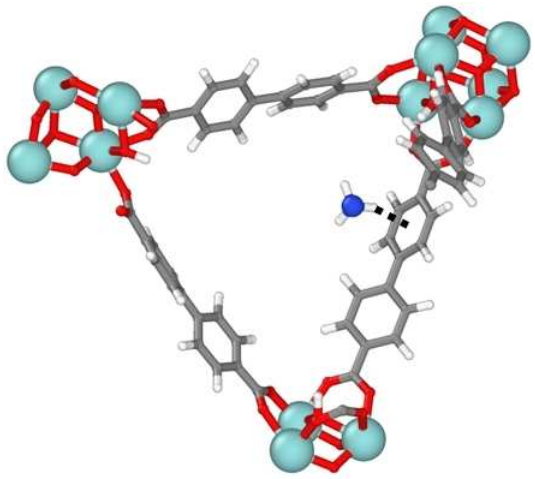

Figure 3. NH–π interaction at a ligand site in UiO-67, obtained through DFT calculations. $\Delta E_{bind} = -11.8\ kJ\,mol^{-1}$, H–$\pi$ interaction distance is 2.61 Å.

MOF framework itself, the steric effects detailed above are not probed. Therefore, the ν(CH) intensity enhancement can be likely attributed to NH–π interactions between NH_3 and linker.

To determine the maximum adsorption capacity of NH_3 in UiO-67, the NH_3 adsorption isotherm for UiO-67 was simulated at 240 K (Figure S9a) and 298 K (Figure S9b). At 240 K, the initial uptake at pressures below about 13 kPa is characterized by a gradual increase in NH_3 loading from zero to 44.2 mg g^{-1}. At 240 K, NH_3 molecules primarily adsorb on the BPDC linkers, likely due to favorable electrostatic interactions at very low pressure (Figure 4, Figures S10–S12). At 1.9 kPa, significant amounts of NH_3 molecules are adsorbed near the BPDC linkers, with lesser amounts at the μ_3–OH groups present in the Zr cluster. The adsorption isotherm at 240 K shows capillary condensation at approximately 20 kPa, beyond which NH_3 saturates the MOF at a liquid-like density. Hence, while NH_3 interacts with the μ_3–OH groups with a higher binding energy, it preferentially binds to the BPDC linkers at low pressure, further reinforcing the presence of NH–π interactions. The reason for NH_3 mainly interacting with the linkers at low pressures is that binding to the μ_3–OH groups is entropically unfavored, since the hydrogen bond results in loss of essentially all translational degrees of freedom, whereas the energetically weaker NH–π interactions allow significant translational and rotational degrees of freedom (see the Supporting Information for details).

The simulated NH_3 adsorption isotherm at 298 K (Figure S9b) shows that at less than 2 bar, NH_3 uptake increases steeply with pressure. At about 2 bar, there is a sudden jump in the NH_3 uptake to 400 mg g^{-1}, indicative of capillary condensation of NH_3 in the pores of UiO-67. We note that previous experimental studies, at 298 K, report a higher NH_3 uptake at 1 bar[18] compared to our computational result. Higher NH_3 uptake in the reported studies can be attributed to the deliberate use of defective MOFs, which contain defects and functional groups designed to enhance NH_3 sorption.

Structural defects in MOFs are known to dictate the balance between their stabilities and chemical reactivities.[9b] Ideally, the node, or secondary building unit (SBU) of a non-defective UiO-67 MOF should contain four μ_3-O groups and Brønsted acid (μ_3–OH group) sites, bound to 12 BPDC linkers coordinated via carboxylate groups and zero Lewis acid sites (undercoordinated Zr^{4+} sites).[32] However, defects, during synthesis, can arise due to several factors which include reaction temperature,[33] reaction time,[34] and modulator choice and concentration.[35] These defects are commonly described as missing linker and missing cluster defects.

Despite many experimental and theoretical studies, an exact molecular picture of defect structure and a precise understanding of their chemistry is unclear. For instance, a few studies report that defect sites are coordinated with H_2O molecules,[36] whereas other studies reveal the presence of modulators at the defect sites.[18b,37] It has been suggested that in the event of a missing linker defect, the coordination of the metal ion and the charge balance is satisfied by H_2O and OH^- ions, respectively.[38] Therefore, it is proposed that the quantification of H_2O capped defect sites is equivalent to quantifying defects capped with hydroxide ions. However, as these isolated species are not involved in hydrogen bonding, their $\nu(OH)_{free}$ is likely masked by the more intense stretching vibration of μ_3–OH groups, making them challenging to distinguish and identify through IR spectroscopy.[39]

The spectra of NH_3 adsorbed upon UiO-67-X MOFs also show the appearance of bands in the 2100–2000 (Figure 5) and 660 cm^{-1} regions (Figure S6), which are neither intrinsic to the MOFs nor to NH_3.[19c,40]

The intensities of the two peaks at around 2110 and 1986 cm^{-1} are an order of magnitude smaller compared to that of $\nu(OH)_{free}$, while the band at approximately 657 cm^{-1} has an intensity comparable to $\nu(OH)_{free}$. We hypothesize that these bands are indicative of the formation of $n NH_3 \cdot H_2O$ complexes,

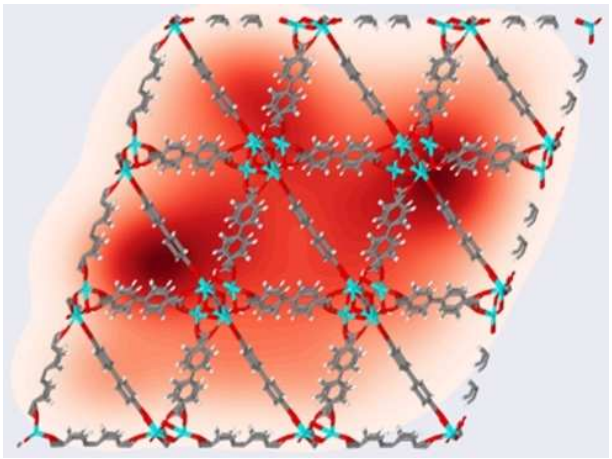

Figure 4. Density probability plot for ammonia in UiO-67 at 1.9 kPa, 240 K. The dark and light red contours represent higher densities and lower densities of ammonia molecules, respectively. Framework atoms: grey: C, white: H, red: O, cyan: Zr.

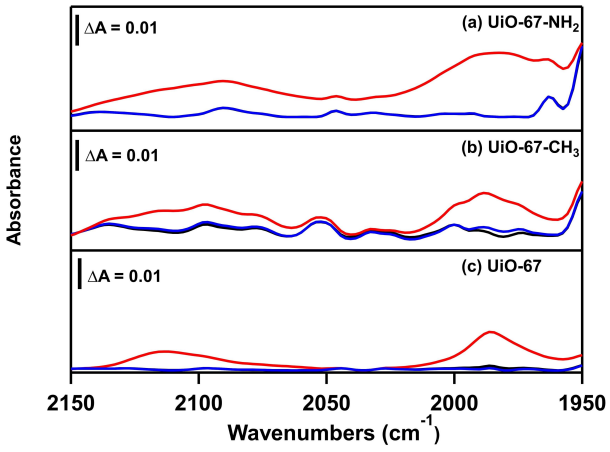

Figure 5. FTIR spectra in the 2150–1950 cm^{-1} region of NH_3 adsorbed upon of (a) UiO-67-NH_2, (b) UiO-67-CH_3, and (c) UiO-67, showing bands of $n NH_3 \cdot H_2O$ clusters: initial spectrum of MOF before exposure (black), 5000 L NH_3 adsorbed on MOF (red), and MOF after thermal treatment (blue). UiO-67, UiO-67-NH_2 activated to 473 K; UiO-67-CH_3 activated to 423 K. Spectra acquired at 100 K.

where the H_2O possibly arises from defects in the MOF.[38,41] The low intensities of these bands suggest that they are a result of interaction with H_2O and not MOF-intrinsic μ_3–OH groups. The presence of a perturbed umbrella mode at around 1038 cm^{-1} (Figure S5) further suggests the formation of $n NH_3 \cdot H_2O$ clusters upon ammonia adsorption.[42] Through DFT calculations, we have found evidence for the stability of such clusters, such as that shown in Figure 6. Thus, it appears that IR spectroscopy of adsorbed NH_3, under controlled conditions, can probe H_2O-terminated defect sites in UiO-67-X MOFs, supported by the relatively small intensity of the $n NH_3 \cdot H_2O$ complex bands compared to other MOF/NH_3 vibrational modes.

Typically, UiO-67 MOFs are thermally treated under vacuum to around 473 K to remove residual solvent, as activation beyond 473 K yields irreversible thermal effects, such as dehydroxylation and structure collapse.[40] Dehydroxylation, which occurs when UiO-67 is heated beyond 473 K, is attributed largely to the release of μ_3–OH from the node through heating.[43] However, since these studies track a mass fragment that can correspond to both μ_3–OH and H_2O (present at missing linker defects), the exact source is unknown. This mass fragment, $m/z = 18$, typically starts to evolve at around 500 K and has a maximum at around 580 K.[40] H_2O in Zr MOFs, if present at a linker defect, is typically spectroscopically hidden due to high intensity of the $\nu(OH)_{free}$ of the μ_3–OH, making degradation product identification ambiguous.[39] NH_3, as seen in Figure 5, is capable of probing H_2O-terminated defects in MOFs. Thus, to determine if these defects are still present after successive thermal activations, NH_3 was adsorbed upon thermally activated UiO-67 ($T_{act} = 523$, 573 K). Due to the similarities between NH_3 adsorption profiles upon UiO-67-X, noted in Figures 1 and 5, and since the node structure is nearly equivalent among them, only adsorption upon thermally treated UiO-67 is investigated.

To determine the presence of missing linker defects, bands indicative of $n NH_3 \cdot H_2O$ clusters were tracked through adsorption of NH_3 upon UiO-67 activated to higher temperatures. The absorbance of the $n NH_3 \cdot H_2O$ cluster bands decreases upon adsorption to the 523 K activated MOF, and nearly vanish upon NH_3 exposure to the 573 K activated MOF (Figures S15–S17). Interestingly, these bands also appear to correlate qualitatively with the reduction of $\nu(OH)_{free}$ intensity at around 3680 cm^{-1} (Figure S18).

In addition to probing the evolution of H_2O-terminated defects within the MOF, NH_3 adsorption on UiO-67 (thermally activated at 523 and 573 K) reveals a change in MOF–NH_3 interactions. On a pristine MOF (Figure 1, Figure S5), NH_3 typically interacts through hydrogen bonding and NH–π interactions. However, as the activation temperature is increased, the intensity of $\nu(OH)_{free}$ reduces to nearly zero (Figure S15) and the intensity of $\nu(NH)_{sym}$ and $\nu(NH)_{asym}$ increases, suggesting NH_3 preferentially adsorbs as a multilayer at 100 K (Figure 7). The interaction with the MOF linker decreases, noted through a reduction in the NH–π interaction intensity, as there is little increase in the MOF intrinsic ν(CH) upon adsorption the MOF thermally activated to 573 K (Figures 7 and S17). This suggests that MOF framework collapse begins at around 523 K, consistent with prior results,[40] which hampers NH_3 access to the MOF interior and results in multilayer adsorption on the exterior crystallite surface, similar to that seen for SWCNTs.[44] NH_3 is thus a versatile probe of the MOF surface and interior, giving insight into defect concentrations and porosity.

As a spectroscopic probe, NH_3 adsorption provides detailed information into the strength and types of acidic sites present in MOFs.[3] In addition to hydrogen bonding with μ_3–OH groups, NH_3 is also capable of interacting with Brønsted/Lewis acid sites present in the MOF through either proton transfer to NH_3 forming NH_4^+ or by donation of a lone pair from NH_3 to electron-deficient Lewis acid sites.[45] NH_3 adsorption on Zr MOFs with a linker similar to that of UiO-67 reveals through IR spectroscopy the formation of NH_4^+ (as a result of proton transfer from an uncoordinated COOH to NH_3), with asymmetric bending modes of NH_4^+, $\delta(NH_4^+)$ situated at around

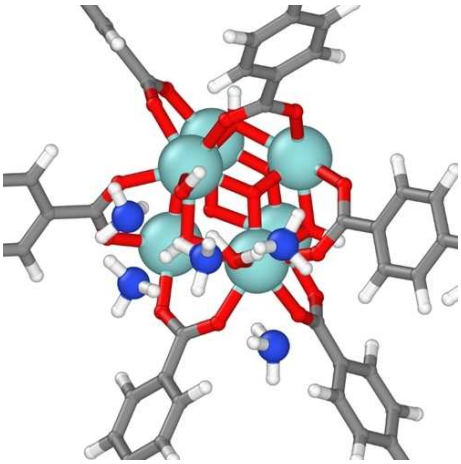

Figure 6. Cluster of five NH_3 molecules at a missing linker defect site capped by H_2O and an OH^- ion, obtained through DFT calculations. $\Delta E_{cluster} = -226$ kJ mol^{-1}; the binding energy of a single NH_3 to the H_2O site, ΔE_{bind}, is approximately -55 kJ mol^{-1}.

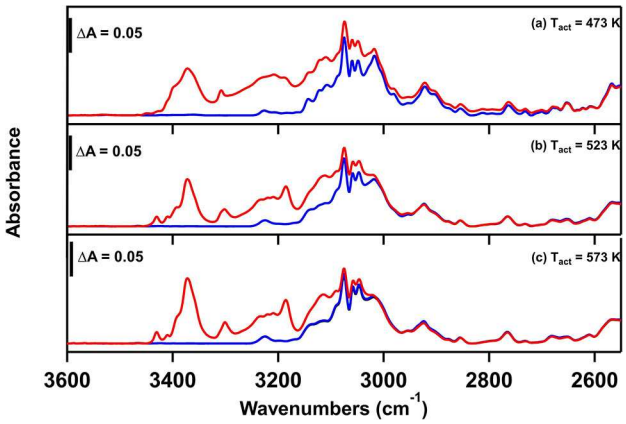

Figure 7. FTIR spectra in 3600–2550 cm^{-1} regions on UiO-67 thermally activated at (a) 473 K, (b) 523 K, (c) 573 K: Initial spectra of MOF before exposure (black), 10000 L NH_3-adsorbed MOF (red), and MOF after thermal treatment (blue). Spectra acquired at 100 K.

1450 cm^{-1}.[45c,46] In the case of porous materials, NH_3 usually reacts with strong Brønsted acid sites, typically free surface hydroxy groups, and forms NH_4^+, with bands situated at around 1480–1380 cm^{-1}.[47] However, our studies (under UHV) show no evidence of NH_3 interacting with Brønsted acidic OH groups, confirmed due to the absence of $\delta(NH_4^+)$ at around 1430 cm^{-1} in Figure S5. Furthermore, the MOFs are stable and do not degrade upon NH_3 sorption. This suggests that NH_3 physisorbs to synthetically pristine UiO-67 in UHV conditions.

Pre- and post-synthetic modification to tune the functional groups and properties of MOFs is a common approach for inducing selectivity or increasing gas uptake.[48] A conventional understanding of gas sorption would be that the uptake of gas molecules occurs via capture in the pores of the MOF/any porous material. However, some studies performed on MOFs elucidate the significance of metal nodes,[49] and linkers on gas sorption.[29]

With FTIR spectroscopy elucidating NH_3-functional group interactions, understanding the mechanisms through which NH_3 binds to MOFs gives insight into strategies to tune MOFs for maximizing the number of binding sites. These NH_3–MOF interactions were identified through TP-IR. Typically, when there are weak interactions between NH_3 and a surface, NH_3 will adsorb as a multilayer, with complete desorption occurring at around 120–130 K (Figure S20).[5,19c,50] Hence, during heating of the adsorbent, the IR absorbance of NH_3-related features is expected to decrease to zero at around 130 K. However, during heating of UiO-67-X MOFs, (Figure 8) the intensity of ν(CH) remains larger than that of the clean MOF up to approximately 270 K. Furthermore, the maximum ν(CH) absorbance occurs at around 165 K (Figure S21). These observations suggest that in addition to μ_3–OH, linkers of UiO-67-X MOFs act as binding sites for NH_3, as suggested by Figure 4. After heating beyond approximately 270 K, the intensity of the ν(CH) recovers to its initial value, suggesting complete removal of NH_3. Thus, in conjunction to hydrogen bonding to OH groups on the node, NH–π interactions between NH_3 and MOFs allow for strong and reversible binding of NH_3 in MOFs.

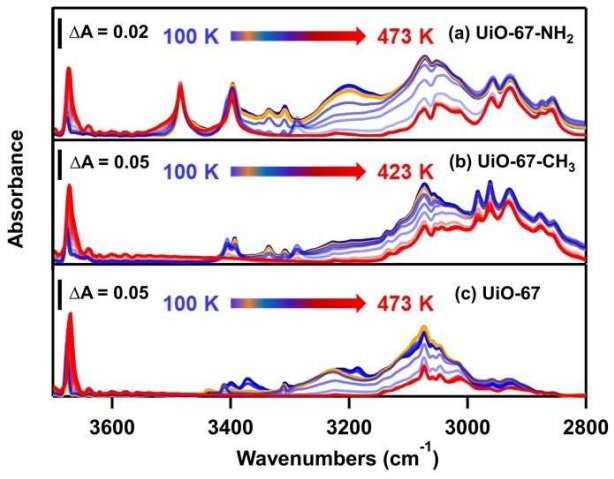

Figure 8. TP-IR spectra in the 3700–2800 cm^{-1} region of (a) UiO-67-NH_2, (b) UiO-67-CH_3, and (c) UiO-67 MOFs during 5000 L NH_3 desorption. Gradient spectra from dark blue to red represent spectra acquired during heating from 100 K to the MOF activation temperature. Orange spectrum is acquired at $T \approx 130$ K, the reported maximum desorption temperature of NH_3 multilayer.

TPD-MS

To determine the type and strength of binding sites available on UiO-67-X for NH_3 adsorption, TPD-MS studies were performed and mass fragment 17 amu ($NH_3^{\cdot+}$, respectively) was monitored while heating the MOFs to their activation temperature. The desorption profiles of NH_3 were observed to be broad and ranging over at least 100 K (Figure 9), which is indicative of NH_3 binding to multiple sites of similar energies.[50] NH_3 was observed to undergo a first order desorption from UiO-67-X, evident by the shared leading edge and the asymmetric shape of the TPD profile for 1000 and 5000 L exposures, seen in Figures S25–S27.[51]

Since the desorption of ammonia from UiO-67-X MOFs is observed to be first order, the Redhead equation [Eq. (2)] is used to obtain approximate desorption energy values.

$$E_{des} = RT_m\left(\ln\frac{\nu T_m}{\beta} - 3.46\right) \quad (2)$$

In Equation (2), E_{des}, T_m, R, β, and ν, are activation energy of desorption [kJ mol^{-1}], temperature at maximum desorption [K], the ideal gas constant (8.314 J mol^{-1} K^{-1}), heating rate (≈ 2 K s^{-1}) and the pre-exponential factor for desorption (assumed to be 10^{13} s^{-1}).[52] See the Supporting Information for the derivation of and other details related to Equation (2). The corresponding E_{des} values for NH_3 desorption from UiO-67-X are summarized in Table 1.

The trend for NH_3 desorption energies (Table 1) is observed to be: UiO-67 < UiO-67-CH_3 < UiO-67-NH_2, supported by positions of the maximum desorption temperatures in Figure 9. For

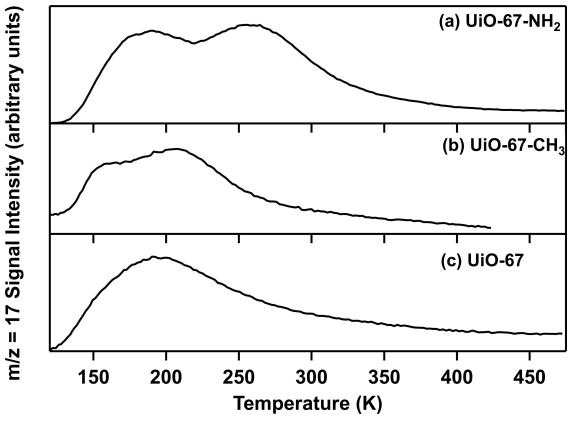

Figure 9. TPD curves tracking molecular ion fragment $m/z = 17$ of NH_3 while MOFs (a) UiO-67-NH_2, (b) UiO-67-CH_3, and (c) UiO-67 were heated from 100 K to activation temperature after 5000 L NH_3 exposure. UiO-67, UiO-67-NH_2 activated to 473 K; UiO-67-CH_3 activated to 423 K. All MOFs were heated at approximately 2 K s^{-1}.

Table 1. Activation energy of desorption for 5000 L NH_3 adsorbed on UiO-67-X. Desorption energies calculated using Equation (2) and averaged over desorption profiles from 3 different samples (Figures S28–S30), reported at the 95% confidence interval.

MOF	E_{des} [kJ mol^{-1}]
UiO-67-NH_2[a]	52.1 ± 3.7
	67.5 ± 1.4
UiO-67-CH_3[b]	40.6 ± 1.8
	55.0 ± 3.4
UiO-67[a]	40.0 ± 5.4
	53.6 ± 6.7

[a] Activated to 473 K. [b] Activated to 423 K.

UiO-67, most NH_3 interactions occur with the MOF linkers and the μ_3–OH (Figure 1). In the case of UiO-67-NH_2, NH_3 hydrogen bonds to not only μ_3–OH but also the amine groups on the linkers, as revealed by decrease in the intensity of $\nu(NH_{free})_{asym}$ intrinsic to the amine-functionalized linker, at around 3485 cm^{-1} upon NH_3 sorption and a recovery in their intensity upon desorption (Figure 1). Since NH_3 hydrogen bonds with different groups on UiO-67-NH_2 (-NH_2 and μ_3–OH groups), there is an increase in the interaction strength, which could result in a higher desorption energy compared to unfunctionalized UiO-67 and UiO-67-CH_3. Interestingly, UiO-67-CH_3, the MOF with non-polar functionalization, has a higher NH_3 desorption energy relative to UiO-67. While this seems counter intuitive, as NH_3 would likely rather interact with a system that has polar moieties, it has been noted that London dispersion forces (LDF) become the primary source of interactions between polar and nonpolar groups in MOFs at low analyte exposures.[53] Thus, the higher affinity towards the non-polar CH_3 groups in UiO-67-CH_3 could be attributed to LDF, consistent with higher desorption energies for NH_3 compared to UiO-67. These energies also suggest physisorption to MOF, as the desorption energies are relatively low compared to energies of NH_3 chemisorption.[47b]

The strength of ammonia binding to porous materials depends on multiple factors, in particular the presence of certain functional groups within the material. When adsorbed upon materials with no NH_3 affinity, NH_3 has a desorption energy of 24 kJ mol^{-1}, which is approximately its sublimation energy.[19c] In the case of porous materials with free COOH groups (strong Brønsted acid sites), the desorption energy for NH_3 is expected to be around 150 kJ mol^{-1}, indicative of chemisorption.[54] The desorption energies obtained here for NH_3 are on the order of 60 kJ mol^{-1}, suggesting strong physisorption between UiO-67-X and NH_3,[55] but not chemisorption of NH_3 to strong Brønsted acidic free COOH, associated with uncoordinated linkers in UiO-67-X. The desorption temperatures, which are smaller than those previously reported under ambient conditions,[18b,56] further suggest physisorption and that the formation of NH_4^+ with μ_3–OH groups on a pristine UiO-67 sample is unlikely under UHV. Thus, the relatively small energies further imply physisorption of NH_3 to synthetically pristine UiO-67-X MOFs.

Conclusion

Fourier-transform infrared (FTIR) spectroscopy and temperature-programmed desorption mass spectrometry (TPD-MS) studies performed under ultrahigh vacuum (UHV) at 100 K suggest strong and reversible binding of NH_3 on UiO-67-X metal-organic frameworks (MOFs). TPD-MS experiments display profiles ranging over at least 100 K, indicative of multiple NH_3 binding sites on MOFs with similar binding energies (≈40–70 kJ mol^{-1}). IR spectroscopy reveals that NH_3 interacts with μ_3–OH on the inorganic node via hydrogen bonding. The increase in ν(CH) intensities and blueshift in NH_3 umbrella motions upon NH_3 sorption suggests NH–π interactions with the benzene moieties of the linker, revealing that UiO-67 linkers are potential binding sites for NH_3. This result is confirmed with density functional theory (DFT) and grand canonical Monte Carlo simulations. The observation of NH–π interactions in the NH_3–MOF system demonstrates the power of UHV studies, which are optimal conditions for pristine MOF-analyte interactions and enable the use of IR spectroscopy as a probe for the identification of binding interactions and sites. Although missing linker defects were undetectable in the IR spectra of the pristine MOFs, bands at approximately 2100, 1980, 1040, and 660 cm^{-1} in the IR spectra, present upon NH_3 sorption, are attributed to NH_3 interacting with H_2O molecules present at the missing linker defect sites through $n NH_3 \cdot H_2O$ cluster formation. DFT calculations show that formation of these clusters is energetically favorable. In addition, the impact of temperature on missing linker defects and MOF structure is illustrated, where NH_3 probes the pore collapse and dehydroxylation of the MOF upon thermal treatment. This demonstrates the versatility of NH_3 for its use to probe structural defects in the MOF. Our studies not only facilitate the structural understanding of MOFs, their defects, and their chemistry in the presence of toxic gases but also provide guidelines for synthesizing stable and efficient MOFs for toxic gas sorption.

Acknowledgements

The authors thank Dr. E. Binaeian for providing experimental NH_3 adsorption isotherm data. This work was partially supported by the Defense Threat Reduction Agency (DTRA) (Grant HDTRA1-16-1-0044) and by the Army Research Office under Cooperative Agreement W911NF-19-2-0187. Calculations were carried out at the University of Pittsburgh's Center for Research Computing. R.P.M. thanks support received from the National Science Foundation (NSF) (Grant no. DUE 1643874) and the Temple University College of Science and Technology Undergraduate Research Program.

Conflict of Interest

The authors declare no conflict of interest.

Keywords: ammonia · defects · density functional theory · infrared spectroscopy · metal-organic frameworks

[1] a) J. B. DeCoste, M. S. Denny Jr., G. W. Peterson, J. J. Mahle, S. M. Cohen, *Chem. Sci.* **2016**, *7*, 2711–2716; b) K. Vikrant, V. Kumar, K. H. Kim, *J. Mater. Chem. A* **2018**, *6*, 22391–22410.
[2] A. Afif, N. Radenahmad, Q. Cheok, S. Shams, J. H. Kim, A. K. Azad, *Renewable Sustainable Energy Rev.* **2016**, *60*, 822–835.
[3] M. Tamura, K. Shimizu, A. Satsuma, *Appl. Catal. A* **2012**, *433*, 135–145.
[4] X. Meng, K. N. Han, *Miner. Process. Extr. Metall. Rev.* **1996**, *16*, 23–61.
[5] X. Feng, S. Irle, H. Witek, K. Morokuma, R. Vidic, E. Borguet, *J. Am. Chem. Soc.* **2005**, *127*, 10533–10538.
[6] W. Fan, X. Wang, X. Zhang, X. Liu, Y. Wang, Z. Kang, F. Dai, B. Xu, R. Wang, D. Sun, *ACS Cent. Sci.* **2019**, *5*, 1261–1268.
[7] T. Zhang, G. Xing, W. Chen, L. Chen, *Mater. Chem. Front.* **2020**, *4*, 332–353.
[8] G. Barin, G. W. Peterson, V. Crocella, J. Xu, K. A. Colwell, A. Nandy, J. A. Reimer, S. Bordiga, J. R. Long, *Chem. Sci.* **2017**, *8*, 4399–4409.
[9] a) M. Kandiah, M. H. Nilsen, S. Usseglio, S. Jakobsen, U. Olsbye, M. Tilset, C. Larabi, E. A. Quadrelli, F. Bonino, K. P. Lillerud, *Chem. Mater.* **2010**, *22*, 6632–6640; b) L. Valenzano, B. Civalleri, S. Chavan, S. Bordiga, M. H. Nilsen, S. Jakobsen, K. P. Lillerud, C. Lamberti, *Chem. Mater.* **2011**, *23*, 1700–1718.
[10] J. H. Cavka, S. Jakobsen, U. Olsbye, N. Guillou, C. Lamberti, S. Bordiga, K. P. Lillerud, *J. Am. Chem. Soc.* **2008**, *130*, 13850–13851.
[11] a) G. E. Cmarik, M. Kim, S. M. Cohen, K. S. Walton, *Langmuir* **2012**, *28*, 15606–15613; b) J. B. DeCoste, T. J. Demasky, M. J. Katz, O. K. Farha, J. T. Hupp, *New J. Chem.* **2015**, *39*, 2396–2399; c) S. Shalini, S. Nandi, A. Justin, R. Maity, R. Vaidhyanathan, *Chem. Commun. (Camb.)* **2018**, *54*, 13472–13490.
[12] a) J. E. Mondloch, M. J. Katz, W. C. Isley, P. Ghosh, P. L. Liao, W. Bury, G. Wagner, M. G. Hall, J. B. DeCoste, G. W. Peterson, R. Q. Snurr, C. J. Cramer, J. T. Hupp, O. K. Farha, *Nat. Mater.* **2015**, *14*, 512–516; b) G. Wang, C. Sharp, A. M. Plonka, Q. Wang, A. I. Frenkel, W. Guo, C. Hill, C. Smith, J. Kollar, D. Troya, J. R. Morris, *J. Phys. Chem. C.* **2017**, *121*, 11261–11272; c) V. S. D. Devulapalli, M. Richard, T.-Y. Luo, M. L. De Souza, N. L. Rosi, E. Borguet, *Dalton Trans.* **2021**, *50*, 3116–3120.
[13] S. Oien-Odegaard, B. Bouchevreau, K. Hylland, L. Wu, R. Blom, C. Grande, U. Olsbye, M. Tilset, K. P. Lillerud, *Inorg. Chem.* **2016**, *55*, 1986–1991.
[14] a) M. J. Katz, A. J. Howarth, P. Z. Moghadam, J. B. DeCoste, R. Q. Snurr, J. T. Hupp, O. K. Farha, *Dalton Trans.* **2016**, *45*, 4150–4153; b) Y. Khabzina, J. Dhainaut, M. Ahlhelm, H. J. Richter, H. Reinsch, N. Stock, D. Farrusseng, *Ind. Eng. Chem. Res.* **2018**, *57*, 8200–8208; c) E. Borfecchia, S. Maurelli, D. Gianolio, E. Groppo, M. Chiesa, F. Bonino, C. Lamberti, *J. Phys. Chem. C.* **2012**, *116*, 19839–19850.
[15] X. Feng, C. Matranga, R. Vidic, E. Borguet, *J. Phys. Chem. B* **2004**, *108*, 19949–19954.
[16] a) J. B. DeCoste, G. W. Peterson, H. Jasuja, T. G. Glover, Y. G. Huang, K. S. Walton, *J. Mater. Chem. A* **2013**, *1*, 5642–5650; b) J. P. Ruffley, I. Goodenough, T. Y. Luo, M. Richard, E. Borguet, N. L. Rosi, J. K. Johnson, *J. Phys. Chem. C.* **2019**, *123*, 19748–19758.
[17] a) M. J. Katz, Z. J. Brown, Y. J. Colón, P. W. Siu, K. A. Scheidt, R. Q. Snurr, J. T. Hupp, O. K. Farha, *Chem. Commun.* **2013**, *49*, 9449–9451; b) B. Wang, H. Huang, X.-L. Lv, Y. Xie, M. Li, J.-R. Li, *Inorg. Chem.* **2014**, *53*, 9254–9259.
[18] a) E. Binaeian, Y. Li, H.-A. Tayebi, D. Yuan, *J. Hazard. Mater.* **2021**, *416*, 125933; b) T. Yoskamtorn, P. Zhao, X. P. Wu, K. Purchase, F. Orlandi, P. Manuel, J. Taylor, Y. Li, S. Day, L. Ye, C. C. Tang, Y. Zhao, S. C. E. Tsang, *J. Am. Chem. Soc.* **2021**, *143*, 3205–3218.
[19] a) K. Manandhar, W. Walkosz, Y. Ren, S. Otani, P. Zapol, M. Trenary, *J. Phys. Chem. C.* **2014**, *118*, 29260–29269; b) K. Hadjiivanov, O. Saur, J. Lamotte, J.-C. Lavalley, *Z. Phys. Chem.* **1994**, *187*, 281–300; c) G. J. Szulczewski, J. M. White, *Surf. Sci.* **1998**, *406*, 194–205.
[20] A. Lubezky, L. Chechelnitsky, M. Folman, *Surf. Sci.* **2000**, *454*, 147–151.
[21] O. S. Binbrek, A. Anderson, *Chem. Phys. Lett.* **1972**, *15*, 421–427.
[22] a) L. Zhang, S. Cui, H. Guo, X. Ma, W. Lu, *Comput. Mater. Sci.* **2016**, *112*, 238–244; b) S. Moribe, Z. J. Chen, S. Alayoglu, Z. H. Syed, T. Islamoglu, O. K. Farha, *ACS Materials Lett.* **2019**, *1*, 476–480; c) C. H. Sharp, J. Abelard, A. M. Plonka, W. W. Guo, C. L. Hill, J. R. Morris, *J. Phys. Chem. C.* **2017**, *121*, 8902–8906; d) A. Davydov, in *Molecular Spectroscopy of Oxide Catalyst Surfaces*; John Wiley and Sons: West Sussex, **2003**, pp. 27–179..
[23] M. D. Ellison, M. J. Crotty, D. Koh, R. L. Spray, K. E. Tate, *J. Phys. Chem. B.* **2004**, *108*, 7938–7943.
[24] a) K. Mizuse, H. Hasegawa, N. Mikami, A. Fujii, *J. Phys. Chem. A* **2010**, *114*, 11060–11069; b) M. Katada, R. Shishido, A. Fujii, *Phys. Chem. Chem. Phys.* **2014**, *16*, 7595–7601; c) M. N. Slipchenko, B. G. Sartakov, A. F. Vilesov, S. S. Xantheas, *J. Phys. Chem. A* **2007**, *111*, 7460–7471.
[25] a) J. L. Bredas, G. B. Street, *J. Chem. Phys.* **1989**, *90*, 7291–7299; b) S. Tsuzuki, K. Honda, T. Uchimaru, M. Mikami, K. Tanabe, *J. Am. Chem. Soc.* **2000**, *122*, 11450–11458.
[26] J. Wanna, J. A. Menapace, E. R. Bernstein, *J. Chem. Phys.* **1986**, *85*, 1795–1805.
[27] a) R. J. Stanley, A. W. Castleman, *J. Chem. Phys.* **1990**, *92*, 5770–5775; b) J. J. Breen, K. Kilgore, W. B. Tzeng, S. Wei, R. G. Keesee, A. W. Castleman, *J. Chem. Phys.* **1989**, *90*, 11–18.
[28] a) D. A. Rodham, S. Suzuki, R. D. Suenram, F. J. Lovas, S. Dasgupta, W. A. Goddard, G. A. Blake, *Nature* **1993**, *362*, 735–737; b) J. A. Menapace, E. R. Bernstein, *J. Phys. Chem.* **2002**, *91*, 2533–2544.
[29] N. L. Rosi, J. Eckert, M. Eddaoudi, D. T. Vodak, J. Kim, M. O'Keeffe, O. M. Yaghi, *Science* **2003**, *300*, 1127–1129.
[30] V. Chandrasekaran, L. Biennier, E. Arunan, D. Talbi, R. Georges, *J. Phys. Chem. A* **2011**, *115*, 11263–11268.
[31] E. Arunan, G. R. Desiraju, R. A. Klein, J. Sadlej, S. Scheiner, I. Alkorta, D. C. Clary, R. H. Crabtree, J. J. Dannenberg, P. Hobza, H. G. Kjaergaard, A. C. Legon, B. Mennucci, D. J. Nesbitt, *Pure Appl. Chem.* **2011**, *83*, 1637–1641.
[32] K. Chakarova, I. Strauss, M. Mihaylov, N. Drenchev, K. Hadjiivanov, *Microporous Mesoporous Mater.* **2019**, *281*, 110–122.
[33] a) Z. Fang, B. Bueken, D. E. De Vos, R. A. Fischer, *Angew. Chem. Int. Ed. Engl.* **2015**, *54*, 7234–7254; b) G. C. Shearer, S. Chavan, J. Ethiraj, J. G. Vitillo, S. Svelle, U. Olsbye, C. Lamberti, S. Bordiga, K. P. Lillerud, *Chem. Mater.* **2014**, *26*, 4068–4071.
[34] H. Wu, Y. S. Chua, V. Krungleviciute, M. Tyagi, P. Chen, T. Yildirim, W. Zhou, *J. Am. Chem. Soc.* **2013**, *135*, 10525–10532.
[35] a) Y. H. Fu, J. Y. Wu, R. F. Du, K. Guo, R. Ma, F. M. Zhang, W. D. Zhu, M. H. Fan, *RSC Adv.* **2019**, *9*, 37733–37738; b) F. Vermoortele, B. Bueken, G. Le Bars, B. Van de Voorde, M. Vandichel, K. Houthoofd, A. Vimont, M. Daturi, M. Waroquier, V. Van Speybroeck, C. Kirschhock, D. E. De Vos, *J. Am. Chem. Soc.* **2013**, *135*, 11465–11468.
[36] a) K. M. Choi, H. J. Jeon, J. K. Kang, O. M. Yaghi, *J. Am. Chem. Soc.* **2011**, *133*, 11920–11923; b) T. H. Park, A. J. Hickman, K. Koh, S. Martin, A. G. Wong-Foy, M. S. Sanford, A. J. Matzger, *J. Am. Chem. Soc.* **2011**, *133*, 20138–20141; c) Y. Zhu, J. Ciston, B. Zheng, X. Miao, C. Czarnik, Y. Pan, R. Sougrat, Z. Lai, C. E. Hsiung, K. Yao, I. Pinnau, M. Pan, Y. Han, *Nat. Mater.* **2017**, *16*, 532–536.
[37] a) S. Ling, B. Slater, *Chem. Sci.* **2016**, *7*, 4706–4712; b) O. V. Gutov, M. Gonzalez Hevia, E. C. Escudero-Adan, A. Shafir, *Inorg. Chem.* **2015**, *54*, 8396–8400.
[38] a) K. Tan, H. Pandey, H. Wang, E. Velasco, K. Y. Wang, H. C. Zhou, J. Li, T. Thonhauser, *J. Am. Chem. Soc.* **2021**, *143*, 6328–6332; b) C. A. Trickett, K. J. Gagnon, S. Lee, F. Gandara, H. B. Burgi, O. M. Yaghi, *Angew. Chem. Int. Ed. Engl.* **2015**, *54*, 11162–11167.
[39] K. I. Hadjiivanov, D. A. Panayotov, M. Y. Mihaylov, E. Z. Ivanova, K. K. Chakarova, S. M. Andonova, N. L. Drenchev, *Chem. Rev.* **2021**, *121*, 1286–1424.
[40] I. Goodenough, V. S. D. Devulapalli, W. Q. Xu, M. C. Boyanich, T. Y. Luo, M. De Souza, M. Richard, N. L. Rosi, E. Borguet, *Chem. Mater.* **2021**, *33*, 910–920.
[41] a) J. E. Bertie, M. M. Morrison, *J. Chem. Phys.* **1980**, *73*, 4832–4837; b) J. E. Bertie, M. R. Shehata, *J. Chem. Phys.* **1985**, *83*, 1449–1456; c) A. Engdahl, B. Nelander, *J. Chem. Phys.* **1989**, *91*, 6604–6612; d) G. Sill, U. Fink, J. R. Ferraro, *J. Chem. Phys.* **1981**, *74*, 997–1000; e) W. J. Zheng, D. Jewitt, R. I. Kaiser, *Astrophys. J. Suppl. Ser.* **2009**, *181*, 53–61; f) J. E. Bertie, M. M. Morrison, *J. Phys. Chem.* **1981**, *74*, 4361–4371.
[42] a) B. Nelander, L. Nord, *J. Phys. Chem.* **1982**, *86*, 4375–4379; b) E. Salli, T. Salmi, L. Halonen, *J. Phys. Chem. A* **2011**, *115*, 11594–11605.
[43] C. Healy, K. M. Patil, B. H. Wilson, L. Hermanspahn, N. C. Harvey-Reid, B. I. Howard, C. Kleinjan, J. Kolien, F. Payet, S. G. Telfer, P. E. Kruger, T. D. Bennett, *Coord. Chem. Rev.* **2020**, *419*, 213388.
[44] D. Kazachkin, Y. Nishimura, S. Irle, K. Morokuma, R. D. Vidic, E. Borguet, *Langmuir* **2008**, *24*, 7848–7856.
[45] a) S. Suganuma, Y. Murakami, J. Ohyama, T. Torikai, K. Okumura, N. Katada, *Catal. Lett.* **2015**, *145*, 1904–1912; b) C. Petit, B. Mendoza, T. J. Bandosz, *Langmuir* **2010**, *26*, 15302–15309; c) Y. W. Chen, X. Zhang, K. K. Ma, Z. J. Chen, X. J. Wang, J. Knapp, S. Alayoglu, F. F. Wang, Q. B. Xia, Z. Li, T. Islamoglu, O. K. Farha, *ACS Appl. Mater. Interfaces* **2019**, *2*, 6098–6102.
[46] S. Bashkova, T. J. Bandosz, *J. Colloid Interface Sci.* **2014**, *417*, 109–114.

[47] a) Y. Yang, M. Faheem, L. Wang, Q. Meng, H. Sha, N. Yang, Y. Yuan, G. Zhu, *ACS Cent. Sci.* **2018**, *4*, 748–754; b) K. Suzuki, T. Noda, N. Katada, M. Niwa, *J. Catal.* **2007**, *250*, 151–160; c) E. Gianotti, V. Dellarocca, L. Marchese, G. Martra, S. Coluccia, T. Maschmeyer, *Phys. Chem. Chem. Phys.* **2002**, *4*, 6109–6115.
[48] Y.-S. Bae, O. K. Farha, J. T. Hupp, R. Q. Snurr, *J. Mater. Chem.* **2009**, *19*, 2131–2134.
[49] Y. Liao, L. Zhang, M. H. Weston, W. Morris, J. T. Hupp, O. K. Farha, *Chem. Commun. (Camb.)* **2017**, *53*, 9376–9379.
[50] T. Suhasaria, J. D. Thrower, H. Zacharias, *Mon. Not. R. Astron. Soc.* **2015**, *454*, 3317–3327.
[51] S. Kwon, R. Vidic, E. Borguet, *Surf. Sci.* **2003**, *522*, 17–26.
[52] a) P. A. Redhead, *Vacuum* **1962**, *12*, 203–211; b) A. M. de Jong, J. W. Niemantsverdriet, *Surf. Sci.* **1990**, *233*, 355–365.
[53] P. Melix, T. Heine, *J. Phys. Chem. C.* **2020**, *124*, 11985–11989.
[54] M. Niwa, K. Suzuki, N. Katada, T. Kanougi, T. Atoguchi, *J. Phys. Chem. B* **2005**, *109*, 18749–18757.
[55] A. S. Al-Dughaither, H. de Lasa, *Ind. Eng. Chem. Res.* **2014**, *53*, 15303–15316.
[56] B. T. Loveless, A. Gyanani, D. S. Muggli, *Appl. Catal. B* **2008**, *84*, 591–597.

Manuscript received: October 15, 2021
Revised manuscript received: October 26, 2021
Accepted manuscript online: November 1, 2021
Version of record online: December 2, 2021